Chapter 6. Electrospray Ionization Ion Mobility Spectrometry of Amino Acids: Ion Mobilities and a Mass-Mobility Correlation

6.1. Abstract

As part of an ongoing effort to explore the utility of high resolution electrospray ionization-ion mobility spectrometry (ESI-IMS) for the detection and identification of organic molecule on other planetary bodies, pursuant to NASA objectives, the reduced ion mobilities of 14 amino acids that have been identified in meteoritic material were determined in both N_2 and CO_2 drift gases. A (12,4) hard-core potential model of the ion-neutral interaction was applied to a combined data set of amino acid mobilities from the present work (abiotic) and an earlier investigation of twenty common biotic amino acids.[1] The model was used to investigate the protonated amino acid mass-mobility correlation in order to extract details of the ion-neutral interaction and to gain insight into the structural details of these ions.

6.2. Introduction

One of the primary objectives in the burgeoning field of astrobiology is the *in situ* detection and identification of organic molecules on the surface of Mars, Europa, and elsewhere. A detailed inventory of organic molecules present on extraterrestrial bodies

will certainly broaden our general understanding of the solar system and may help elucidate questions regarding the origin of life on Earth and the possibility of life elsewhere in the Universe. These intriguing possibilities have prompted a flurry of activity in terms of investigating various means of performing such detection and identification. As such, this work is intended to further examine the feasibility of high-resolution electrospray ionization-ion mobility spectrometry (ESI-IMS) as a tool for *in situ* analysis of organic compounds.[1,2]

Amino acids found in the terrestrial environment are generally associated with biotic processes as part of more complex molecules, such as peptides and proteins, but are also found as individual molecules as a result of the hydrolyses of biopolymers. Outside the terrestrial environment, amino acids can be formed by abiotic processes in various space and extraterrestrial environments as demonstrated by their positive identification in carbonaceous meteoritic infall, including the Murchison CM2 meteorite.[3,4,5] Specifically, analysis of the Murchison meteorite identified 33 amino acids which have no known biotic source, 11 amino acids which have limited distribution and 8 amino acids which readily occur in terrestrial proteins[6]. The fact that amino acids play an important role in terrestrial life and that they are believed to be prevalent outside the terrestrial environment makes them prime targets for identification on other planetary bodies.

In the present investigation, ESI-IMS (positive mode) was used to measure the reduced mobilities of 14 abiotic amino acids in N_2 and CO_2 drift gases. The 14 amino acids studied were chosen from a list of amino acids identified in the Murchison CM2 meteorite, which is an indication of abiotic origin.[3-6] With this investigation, a substantial database of amino acid ion mobility constants (20 common biotic[1] and 14 abiotic-present

work) is now available for use in modeling efforts and to identify IMS peaks in complex field samples.

Throughout the history of ion mobility spectrometry (plasma chromatography), many attempts have been made to draw correlations between an ion's mobility and its mass. In 1973, Griffin et al.[7] performed a review of experimental and theoretical ion mobility data and concluded that mass estimates of structurally unrelated compounds based on ion mobility alone, could not be made to an accuracy of better than 20% and should therefore be discouraged. However, they also concluded that this error could be lowered by as much as an order of magnitude (i.e., 2%) for a series of structurally related compounds. It was further concluded that within a limited series of related compounds, ion mobilities were characteristic of the sample material and could be used to identify unknown compounds. Ultimately, a tandem IMS-mass spectrometer instrument (IMS-MS), yielding both the mobility and mass of an ion, could place an unknown ion on the mass-mobility plane. By comparing an ion's location on this plane with predetermined regions characteristic of various compound classifications (i.e., known mass-mobility correlation curves), one could identify the family of compounds to which the unknown belongs in a manner similar to the retention times in two dimensional gas chromatography. Such an ability would be of tremendous value if a tandem IMS-MS system was used to analyze unknown samples in a complex chemical environment.

Before such a scenario can become a reality, a number of issues need to be addressed. A mobility-mass database would have to be accumulated for a given drift gas and then differentiated into groups of structurally related compounds. As a matter of practical interest, it is impossible to accumulate an exhaustive database of mass and mobility. It is

therefore desirable to develop analytical predictions to extrapolate and interpolate over unmeasured regions of the mass-mobility plane.

Previous works have shown that the mass-mobility correlation can be accurately modeled for molecules in a homologous series. Berant and Karpas[8,9] demonstrated an ability to accurately model the mass-mobility correlation of compounds in three distinct classifications (acetyls, aromatic amines, and aliphatic amines) drifting in He, N_2, air, Ar, CO_2 and SF_6. More recently, Illenseer and Löhmannsröben[10] investigated the mass-mobility correlation of aromatics (from benzene to C_{60} fullerene). In this work, the amino acid mass-mobility correlation is modeled based on the mobilities (and masses) of biotic amino acids reported by Beegle et al.[1] and the abiotic amino acid mobilities determined in the present work. The model was used to investigate the validity of an amino acid mass-mobility correlation, extract details of the ion-neutral interaction and to obtain insights into the structural details of these ions. Previous work[1,11] has shown that ESI of amino acids in the positive mode results overwhelmingly in singly charged, protonated amino acid ions. Therefore, this is assumed to be the case in the above discussion and throughout this work.

6.3. Experimental

The 14 abiotic amino acids studied here were obtained from Sigma Chemical Company (St. Louis, MO) and were used without further purification. All solvents (water, acetic acid and methanol) were HPLC grade and were purchased from J. T. Baker (Pillipsburgh, NJ). Samples were prepared by weighing out known quantities of amino acids and then dissolving them in a solvent solution consisting of 47.5% water, 47.5% methanol and 5%

acetic acid by volume. The sample concentrations were approximately 10 parts per million (ppm) of amino acid to solvent by weight.

The ESI-IMS instrument used in this investigation was based on designs previously described by Hill and co-workers.[11,12] The drift length of the ion mobility spectrometer was 13.5 cm and was operated in the positive mode. Drift voltages which provided the maximum resolving power in N_2 and CO_2 were determined empirically. These voltages, 5580 V in N_2 and 7980 V in CO_2, corresponding to electric field strengths of 413 V/cm and 591 V/cm, respectively, were employed as appropriate.

The drift tube was held at a constant temperature of 500 K by means of an aluminum heating jacket that enclosed the entire length of the desolvation and drift regions. Two thermocouples were located along the length of the heating jacket and were used to provide feedback to two heater controllers which maintained a constant, preprogrammed temperature. In order to ensure that the temperature of the heating jacket accurately represented the temperature within the spectrometer volume, the drift gas was heated by passing it through a stainless steel tube held in direct thermal contact with the heating jacket, prior to its introduction into the drift cell.

All measurements were made at the local atmospheric pressure (~730 torr at JPL) while a counter flow of the preheated drift gas was introduced at the detection end of the drift region at a flow rate of ~800 mL/min for N_2 and ~1100 mL/min for CO_2. The differences in these flow rates can be attributed to the open nature of the IMS cell. The higher CO_2 flow was required to ensure complete displacement of the drift volume with CO_2. Over the course of the measurements, the pressure was seen to vary between 727 and 732 torr as monitored with a 1000 torr head capacitance manometer. As such, an average value of 730 torr was used in all calculations of the reduced mobility.

The sample solution was delivered by an Eldex Micropro liquid chromatography pump at a flow rate of 5 μl/min into the metal electrospray needle which was held 3.5 kV above the entrance to the desolvation region of the spectrometer. In order to prevent solvent from evaporating in the needle, the needle was cooled with a flow of room temperature gas (same species as the drift gas; ~150 ml/min).

Ions were introduced into the drift region by toggling the ion gate "open," for 0.2 ms. Signals collected at the Faraday cup were amplified by a factor of 10^9 (Stanford Research Systems Model SR570 low-noise current preamplifier) and recorded as a function of drift time in 0.02 ms wide channels. Typically, 1000 individual 0 to 20 ms scans were averaged to produce the final spectra used in the analysis. Resolution of the instrument was found to be ~0.36 ms full width at half maximum (FWHM). Reduced ion mobilities, K_0, were determined from the recorded spectra and the experimental parameters according to the usual relation,

$$K_0 = \left(\frac{273\,\mathrm{K}}{T}\right)\left(\frac{P}{760\,\mathrm{Torr}}\right)\frac{L^2}{Vt}, \qquad (1)$$

where V is the voltage drop across the drift region, L is the drift length, t is the drift time, P is the pressure and T is the temperature. With the above parameters expressed in units of V, cm, s, torr and K, respectively, equation (1) gave the reduced mobility in the typical units of $cm^2\,V^{-1}s^{-1}$.

Before proceeding with this investigation, reduced mobilities were determined for three amino acids chosen to cover the range of ion masses investigated in this study. These mobilities were compared to data reported in the literature to assess the quality and reliability of the current apparatus and procedures. Specifically, the reduced mobilities of protonated serine, phenylalanine, and tryptophan ions were measured in N_2 and compared

to the corresponding mobilities reported by Asbury and Hill[11] and Beegle et al.[1] Both the Asbury and Hill[11] and Beegle et al.[1] data were reported at 523 K. Therefore, to ensure a direct comparison, the test measurements were conducted with the temperature of the drift cell elevated to 523 K. Furthermore, an electric field strength of 280 V/cm corresponding to a field strength to gas density ratio (i.e., E/N) of ~2 Td was chosen to ensure that the spectrometer was operating under low-field conditions during these validation measurements (i.e., mobilities were independent of the electric field). Comparisons of the data showed agreement within the estimated experimental uncertainty of ~5% and thereby confirmed the accuracy of the apparatus and measurement procedures.

As stated earlier, electric field strengths of 413 and 591 V/cm were employed during the current measurements of abiotic amino acid mobilities. To ensure that the spectrometer was operating under low-field conditions at these field strengths, a series of test measurements were conducted. Reduced mobilities were determined for serine, phenylalanine, and tryptophan at 500 K with field strengths of 413 and 591 V/cm in N_2 and CO_2, respectively. The measurements were then repeated with reduced field strengths of 280 and 325 V/cm in N_2 and CO_2, respectively. Agreement was seen between all corresponding mobilities within experimental uncertainties (~5%) with a maximum observed deviation of 2%. These results verified that the current measurements were made at sufficiently low electric fields to avoid any dependence of the measured mobilities on the electric field. In other words, the spectrometer was indeed operating under low-field conditions throughout the course of this investigation.

6.4. Modeling

6.4.1. Theoretical Approach. The equation governing gas-phase ion transportation in an electric field is given by Revercomb and Mason[13] as

$$K = \frac{3q}{16N}\left(\frac{2\pi}{\mu kT}\right)^{1/2}\frac{1}{\Omega}, \qquad (2)$$

where K is the ion mobility, N is the number density of the drift gas atoms/molecules, q is the charge on the ion, μ is the reduced mass, k is the Boltzmann constant, T is the temperature in the drift region, and Ω is the collision cross section. Therefore, differences in the mobilities of ions drifting under identical conditions (i.e., temperature, pressure) are a result of the explicit mass dependence in μ and the collision cross section. The expression for the ion mobility given in equation (2) represents the first approximation of a rigorous kinetic theory for low field conditions. Corrections to this equation are generally taken into account by including a factor of $(1+\beta)$ in the numerator. However, for ion masses which are greater than or equal to the mass of the neutral molecule, the value of β is less than 0.02[13]. Since this condition holds for all scenarios considered in the present work, the $(1+\beta)$ correction factor has been omitted.

The cross section contains all the information regarding the ion-neutral interaction. In terms of calculation, it is convenient to write the cross section in terms of a dimensionless collision integral for diffusion, $\Omega^{(1,1)*}$, normalized to unity for rigid spheres with a summed radii of r_m:

$$\Omega = \pi r_m^2 \Omega^{(1,1)*} \quad . \qquad (3)$$

Given the interaction potential, $\Omega^{(1,1)*}$ can be calculated as a function of temperature through three successive integrations over collision trajectories, impact parameters and energy[14,15].

In practice, a variety of models are used to approximate the cross section based on interaction potentials with various attractive and repulsive terms. In the absence of a permanent dipole or quadupole moment in the neutral, all these potentials share a common long-range attractive term ($\sim r^{-4}$). This *polarization potential* is due to the interaction between the ionic charge and the moment it induces in the neutral and is given by

$$V_{pol}(r) = -\frac{q^2\alpha}{2r^4}, \tag{4}$$

where r is the separation between the geometric centers of the ion and neutral and α is the neutral polarizability. Since this is the component that dominates at low energies (i.e., in the limit of $T \rightarrow 0$ K), all mobilities approach a common low energy limit[16], i.e., the polarization limit:

$$K_{pol} \equiv K(T \rightarrow 0\,\mathrm{K}) = \frac{13.853\,\mathrm{cm^2V^{-1}s^{-1}}}{(\alpha\mu)^{1/2}}, \tag{5}$$

where K_{pol} is at standard gas density and α and μ are in units of Å^3 and amu, respectively. For the purposes of this study, the so-called (12,4) hard-core potential, which has proven sufficient to accurately model experimental data in the past,[8,9,17,18] has been chosen to represent the ion-neutral interaction. This potential takes the form

$$V(r) = \frac{\varepsilon}{2}\left\{\left(\frac{r_m - a}{r - a}\right)^{12} - 3\left(\frac{r_m - a}{r - a}\right)^{4}\right\}, \tag{6}$$

where ε is the depth of the potential well, r is as before, r_m is the value of r at the potential minimum, and a is the location of the ionic center of charge measured from the geometrical center of the ion (see Figure 1). For a given neutral species, the depth of the

potential well is ion dependent. However, it can be fixed in terms of the other relevant parameters by requiring that the coefficient of the r^{-4} term equal the known polarization potential coefficient (equation 4). This requirement ensures that the resulting ion mobilities are in agreement with the $T \rightarrow 0$ K polarization limit and gives the potential depth as

$$\varepsilon = \frac{q^2 \alpha}{3 r_m^4 (1 - a^*)^4}, \tag{7}$$

where the dimensionless parameter $a^* = a/r_m$ has been introduced. Now that the potential is defined, the dimensionless collision cross section can be calculated as discussed above. Tabulations of $\Omega^{(1,1)^*}$ can be found in the literature[15] for the (12,4) hard-core potential as functions of a^* and the dimensionless temperature, T^*, given by

$$T^* = \frac{kT}{\varepsilon} = \frac{3kTr_m^4 (1 - a^*)^4}{q^2 \alpha}. \tag{8}$$

If the ions and neutral molecules are represented as spherical volumes of uniform mass, then their radii are proportional to the cubed root of their masses and a considerable simplification is achieved. With this assumption, r_m can be expressed as the sum of the ion and neutral radii in the following manner

$$r_m = r_0 \left[1 + \delta \left(\frac{m}{M} \right)^{1/3} \right], \tag{9}$$

where δ^3 is the relative neutral to ion density ratio, which is assumed to be unity, and r_0 is the neutral radius. It has been empirically determined that an improvement in the model's performance can be made by introducing a mass dependent correction term into the expression for r_m of the form $m\gamma^8$;

Figure 1. A schematic plot of the (12,4) hard-core potential, *V(r)*, as a function of the ion-neutral center of mass separation, *r*, is shown as a soil line. Circles on the plot show spherical representations of the ion and neutral at $r = r_m$, the location of the potential minimum of depth ε. Solid dots indicate the position of the ion and neutral centers of mass. An open dot indicates the position of the ion's center of charge. The neutral radius, r_0, is also indicated.

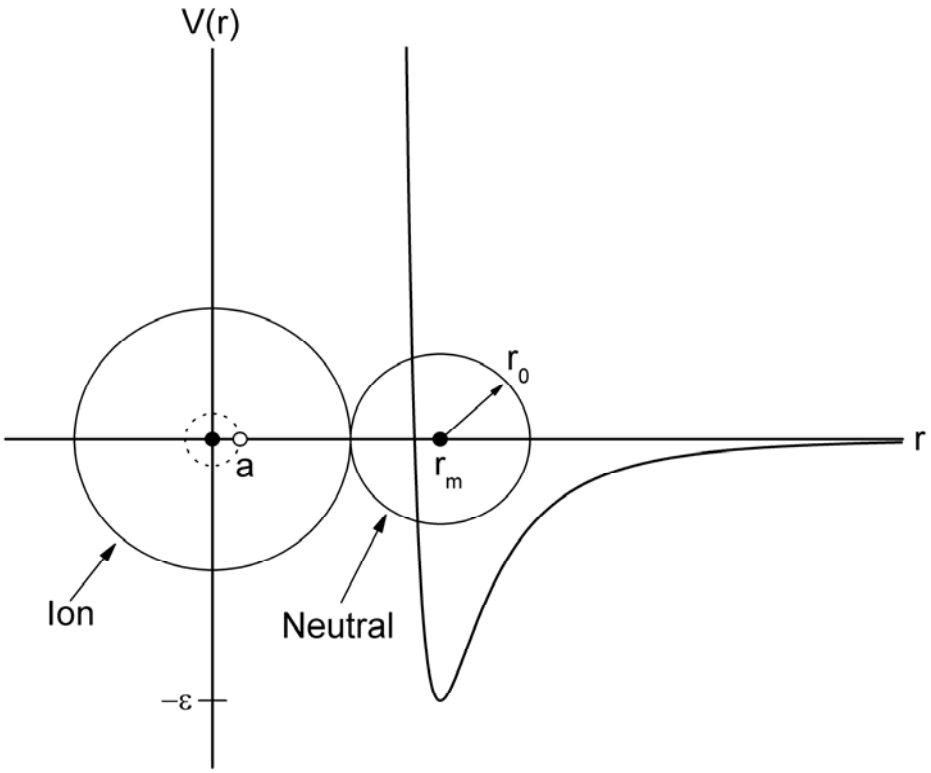
V(r)
r
a
r_m
r_0
Ion
Neutral
−ε

$$r_m = (r_0 + m\gamma)\left[1 + \left(\frac{m}{M}\right)^{1/3}\right]. \qquad (10)$$

The expression for gas phase mobility can be rearranged, substituting the appropriate constants to give

$$K_0^{-1} = (1.697 \times 10^{-4})(\mu T)^{1/2}\, r_m{}^2\, \Omega^{(1,1)*} \ , \qquad (11)$$

which yields reduced ion mobilities in units of $cm^2\ V^{-1}\ s^{-1}$ with r_m in Å (equation 10; calculated with r_0 in Å, m and M in amu and γ in units of Å/amu). Since, the mobility data under scrutiny in this investigation were obtained in a drift cell at 500 K, no correction or allowance was made to account for an increase in effective ion mass due to clustering of drift gas molecules and the primary ions of interest[17].

6.4.2. The Amino Acid Data Sample. As indicated earlier, the amino acid mobility data measured in this study were combined with our earlier work on biotic amino acids[1] for the purposes of the present mass-mobility analysis. This was done to increase the sample size upon which the analysis was performed and thereby improve the statistical accuracy of the results. However, the Beegle et al.[1] data were measured at 523 K while the present data were measured at 500 K. Therefore, some justification for considering these data as a self-consistent sample is required before proceeding.

The dependence of ion mobility on temperature has been examined in the literature[17] and has been reviewed in detail by Eiceman and Karpas.[19] This dependence is manifest in eqs 2 and 11 as the temperature not only appears directly in these expressions for ion mobility but through the temperature dependence of $\Omega^{(1,1)*}$. Furthermore, the temperature can affect ion mobility through clustering of neutral drift molecules with the ion of interest. However, as alluded to earlier, clustering is not significant at the temperatures in question (500 and 523 K)[17,19] and, therefore, is not relevant to the current discussion.

Equation 11 shows that K_0^{-1} is proportional to $T^{1/2}\Omega^{(1,1)*}$. As such, the behavior of $\Omega^{(1,1)*}$, which is determined by the nature of the ion-neutral interaction potential, must be known to describe the exact nature of the temperature dependence of K_0^{-1}. If a hard sphere model is assumed, $\Omega^{(1,1)*} = 1$ and K_0^{-1} is proportional to $T^{1/2}$. This in turn implies that K_0^{-1} will vary on the order of 2.3% over the relevant 500-523 K temperature range. On the other hand, in the Langevin model,[20] which assumes the ion-neutral interaction is due solely to the polarization potential (eq 4), $\Omega^{(1,1)*}$ varies as $T^{-1/2}$ resulting in a reduced mobility that is independent of temperature.

To develop a better predication for the temperature dependence of the reduced mobility over the relevant temperature range (500-523 K), $T^{1/2}\Omega^{(1,1)*}$ was calculated for ions drifting in N_2 and CO_2 assuming a (12,4) hard-core potential. To proceed, estimates of a^*, γ, and r_0 were required. These estimates were made based on the results of Karpas and Berant,[9] who used a (12,4) hard-core potential to analyze the mobilities of aliphatic amines in N_2 and CO_2 as a function of ion mass. These analyses gave values of $a^* = 0.2$ (0.3), $\gamma = 0.0021$ Å/amu (0.0018 Å/amu), and $r_0 = 2.29$ Å (2.60 Å) for protonated aliphatic amines in N_2 (CO_2). For lack of a better means of predicting the values of a^* appropriate for amino acid ions drifting in N_2 and CO_2, the average of the Karpas and Berant[9] a^* values listed above was used in these calculations, i.e.,, $a^* = 0.25$. As seen in the discussion prior to eq 10, γ represents an empirical refinement to the expression for r_m and, in practice, is generally small.[8,9,17,18] Therefore, γ was taken to be zero. The values of r_0 determined by Karpas and Berant[9] for N_2 and CO_2 were used to estimate the temperature dependence as appropriate.

T^* was calculated via eqs 8 and 10 over the range of ion masses considered in this work (76-205 amu) at T = 500 and 523 K for ions drifting in N_2 and CO_2, using the estimates for a^*,γ, and r_0 discussed above and the appropriate values for M and α. Values of $\Omega^{(1,1)^*}$ were then determined from literature tabulations[15] for the corresponding values of T^*. The differences in $T^{1/2}\Omega^{(1,1)^*}$ at T = 500 and 523 K were then calculated as a function of ion mass for each drift gas. The results of these calculations showed a maximum predicted variation of 1.2%. A variation of this magnitude is below the resolution limit of the current apparatus (~5%) and would imply that combining the data sets for the mass-mobility analysis as proposed would be legitimate.

To verify that the variation was indeed below the resolution limit of the instrument, the reduced mobilities of serine, phenylalanine, and tryptophan were measured in N_2 and CO_2, using the current procedures at 500 K, and compared to the 523 K results of Beegle et al.[1] These comparisons showed a maximum deviation of 3% between reduced mobilities of a given ion measured at each temperature. This confirmed that the current apparatus was not capable of resolving any difference between reduced ion mobilities over the 500-523 K temperature range. As a result, it was concluded that the amalgamation of the current data set with the Beegle et al.[1] data was a legitimate means of increasing the sample size and thereby increasing the statistical accuracy of the amino acid mass-mobility correlation analysis.

6.4.3. Fitting Procedure. Equation (11) was fit to each available set of amino acid mobility data (in N_2 and CO_2; the combined data set from the present study and that of Beegle et al.[1]) using a non-linear least squares fitting procedure. Parameters of the fit were the neutral radius, r_0, the dimensionless charge location, a^*, and the correction factor, γ, with the ion mass, m, being the independent variable. Calculated values for

$\Omega^{(1,1)*}$ from the literature[15] were used along with the appropriate ion and neutral masses (reduced mass), temperature (T = 500 K) and polarizability (α = 1.740 and 2.911 for N_2 and CO_2, respectively[19]). As mentioned previously, the amino acids were assumed to be singly ionized via the addition of a proton in the electrospray process.[1,11] Therefore, q was taken to be $e = 1.6\times10^{-19}$C and the masses of the measured ions were incremented by 1 amu accordingly. Since values of $\Omega^{(1,1)*}$ were found in tabulations as a function of discrete T^* and a^* values, the fitting procedure proceeded as follows.

A discrete a^* was taken for which $\Omega^{(1,1)*}$ values were available,[15] and T^* and r_m were calculated based on an initial guess of r_0 and γ. Given the calculated value for T^*, the appropriate $\Omega^{(1,1)*}$ was interpolated from the literature tabulation. The interpolation procedure was accomplished by fitting a third order exponential decay of the form

$$y = A_0 + A_1 e^{-(x-x_0)/\tau_1} + A_2 e^{-(x-x_0)/\tau_2} + A_3 e^{-(x-x_0)/\tau_3} \qquad (12)$$

to the $\Omega^{(1,1)*}$ data for the given value of a^*. In order to maximize the quality of the interpolation procedure, the fit was limited to a small range of relevant T^* values (T^*=1-20) as determined from similar studies;[8,9] the appropriateness of this range was verified by the final fitting results. All such fits were seen to give coefficients of determination, R^2, approximately equal to unity, and thereby provided an excellent means of interpolation (Figure 2). Once all the required quantities were at hand, K_0^{-1} was calculated as a function of ion mass. The parameters r_0 and γ were adjusted to provide the best fit to the experimental K_0^{-1} data points (i.e., minimize the reduced Chi squared, χ_v^2). This procedure was repeated for each available a^*. The set of parameters, a^*, r_0 and γ, that produced the smallest χ_v^2 were chosen as the best fit (or equivalently, the fit with R^2 closest to unity).

Figure 2. An example of the fits to the $\Omega^{(1,1)*}$ values tabulated by Mason et al.[15] used to interpolate between T^* entries. Specifically, the result of fitting a third order exponential decay (solid line) to the $a^* = 0.2$ data set (solid circles) is shown ($\chi_\nu^2 = 2.34\times10^{-7}$, $R^2 \cong 1$).

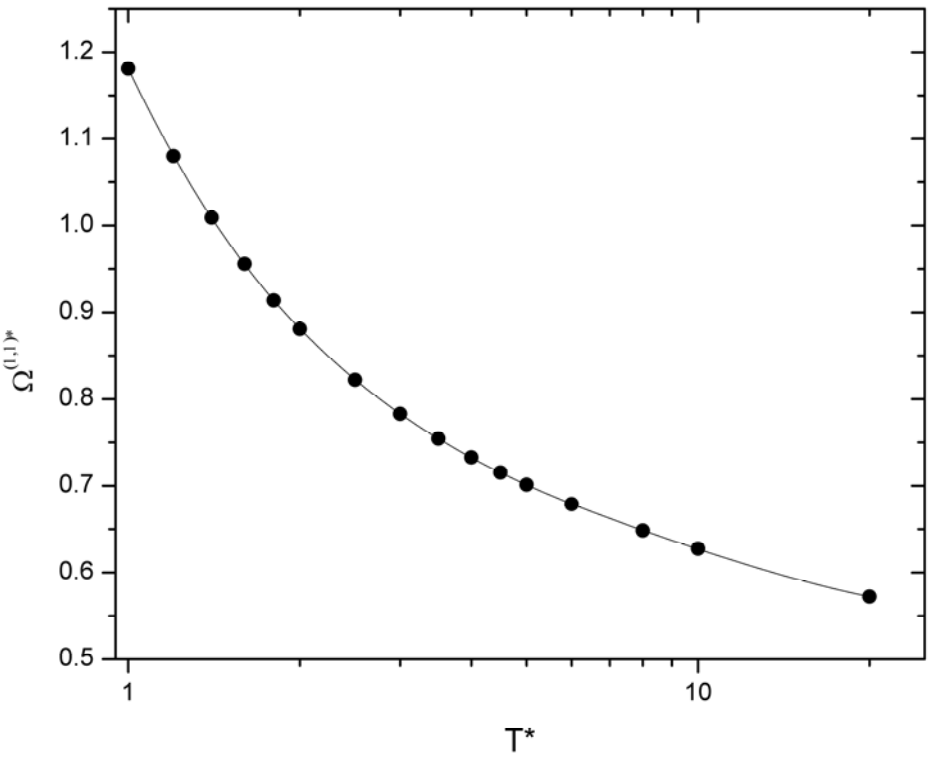
1.2
1.1
1.0
0.9
0.8
0.7
0.6
0.5
$\Omega^{(1,1)*}$
1
10
T*

6.5. Results and Discussion

IMS spectra were obtained as described above. After the amino acid features were identified, drift times were determined by the location of the peak maxima. Measured drift times and reduced ion mobilities in both N_2 and CO_2 drift gasses for the 14 abiotic amino acids chosen for this study are listed in Table 1. Figure 3 shows example spectra taken with pure solvent being introduced to the electrospray needle and with 10 ppm of L-norleucine dissolved in the solvent. These spectra are characteristic of those considered in this work.

Of note are the demonstrated dependences of the ion mobilities and, therefore, ion separability on the drift gas species. For example, in CO_2, four of the lightest amino acids, sarcosine (90 amu), β-alanine (90 amu), DL-β-amino-n-butyric acid (104 amu) and α-aminoisobutyric acid (104 amu), covered a range in drift times of only 0.08 ms. Therefore, a mixture of these species could not be resolved the current arrangement (FWHM ~0.36 ms). However, in N_2, these same amino acids recorded drift times of 8.6, 9.4, 9.7, and 10.1 ms, respectively, and could be resolved. These results are consistent with previous studies that have shown that ion separation can be drastically improved through a judicious choice of drift gas.[1, 2, 9, 20, 21]

Figures 4 and 5 show plots of K_0^{-1} versus ion mass for protonated amino acids drifting in N_2 and CO_2, respectively. The plots include both the current abiotic data and the biotic data from Beegle et al.[1] Beegle et al.[1] present reduced mobilities in N_2 measured with two different drift voltages. Therefore, the averages of these values were employed here. A line representing the best fit of the model to the plotted data is also shown in these two figures. Table 2 gives a tabulation of modeled amino acid mobilites in N_2 and CO_2 at masses corresponding to the ions considered in this work. Included in Table 2 are the

Table 1. Drift times and reduced mobilities of abiotic amino acids in N_2 and CO_2 drift gases

Amino acid	Chemical Formula	MW[a]	N_2		CO_2	
			DT[b]	K_0 [c]	DT[b]	K_0 [c]
sarcosine	$C_3H_7NO_2$	90	8.64	1.982	11.50	1.042
β-alanine	$C_3H_7NO_2$	90	9.40	1.821	11.56	1.037
N-methyl-DL-alanine	$C_4H_9NO_2$	104	9.50	1.802	11.26	1.064
DL-β-amino-n-butyric acid	$C_4H_9NO_2$	104	9.68	1.769	11.54	1.039
γ-amino-n-butyric acid	$C_4H_9NO_2$	104	9.68	1.769	11.30	1.061
DL-α-amino-n-butyric acid	$C_4H_9NO_2$	104	9.94	1.722	11.96	1.002
α-aminoisobutyric acid	$C_4H_9NO_2$	104	10.10	1.695	11.48	1.044
L-norvaline	$C_5H_{11}NO_2$	118	10.66	1.606	12.30	0.974
1-amino-1-cyclopetanecarboxylic acid	$C_6H_{11}NO_2$	130	10.84	1.579	12.10	0.990
DL-pipecolinic acid	$C_6H_{11}NO_2$	130	10.40	1.646	12.06	0.994
L-norleucine	$C_6H_{13}NO_2$	132	11.32	1.512	12.62	0.950
α -methyl-DL-aspartic acid	$C_5H_9NO_4$	148	10.94	1.565	12.42	0.965
N-methyl-DL-aspartic acid	$C_5H_9NO_4$	148	10.80	1.585	13.10	0.915
DL-α-aminopimelic acid	$C_7H_{13}NO_4$	176	11.82	1.449	13.42	0.893

[a] Protonated molecular weight (amu). [b] Drift time (ms). [c] Reduced mobility ($cm^2 V^{-1} s^{-1}$).

Figure 3. Examples of the ion mobility spectra taken in this study. Shown are two spectra taken in N_2. The dash curve is a spectrum taken with pure solvent being introduced to the electrospray needle while the solid curve is a spectrum of solvent and 10 ppm of L-norleucine. The two spectra were smoothed (10 point adjacent averaging) and shifted in intensity by an additive constant to avoid overlap. The L-norleucine feature is indicated in the figure. The un-labeled features correspond to ionized solvent (water, methanol and acetic acid) and atmospheric constituents ionized through proton transfer (due to the open nature of the ESI-IMS instrument).

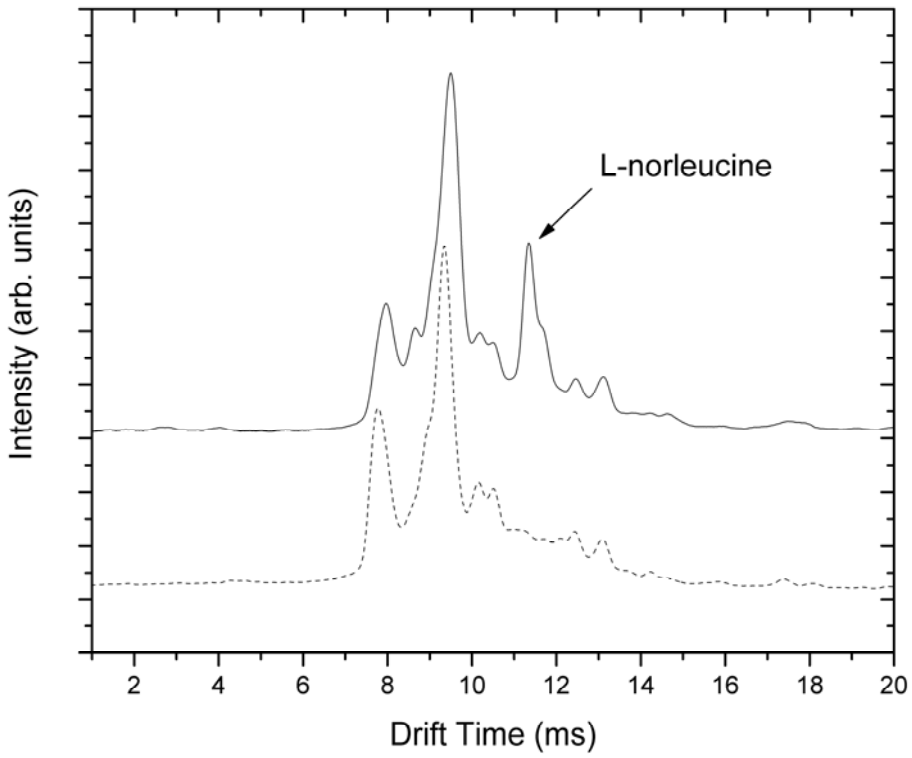
L-norleucine
Intensity (arb. units)
2
4
6
8
10
12
14
16
18
20
Drift Time (ms)

Figure 4. Plot of K_0^{-1} for protonated amino acids drifting in N_2 versus ion mass. The present abiotic data are shown as solid circles along with the biotic amino acid data of Beegle et al.[1] which are shown as open circles. The fit of the (12,4) hard-core potential model to the combined data set is shown as a solid line (r_0 = 2.56 Å, γ=0.0004 Å/amu, a^* = 0.2).

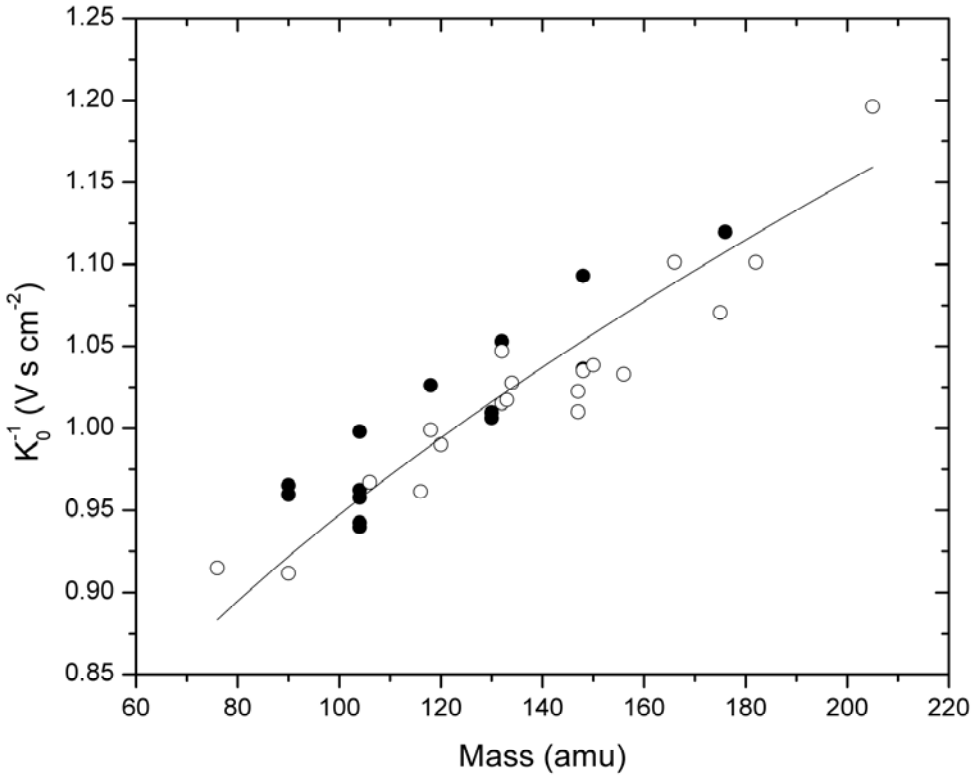
1.25
1.20
1.15
1.10
1.05
1.00
0.95
0.90
0.85
K_0^{-1} (V s cm^{-2})
60
80
100
120
140
160
180
200
220
Mass (amu)

Figure 5. Plot of K_0^{-1} for protonated amino acids drifting in CO_2 versus ion mass. The present abiotic data are shown as solid circles along with the biotic amino acid data of Beegle et al.[1] which are shown as open circles. The fit of the (12,4) hard-core potential model to the combined data set is shown as a solid line (r_0 = 2.92 Å, γ = 0.0000 Å/amu, a^* = 0.3).

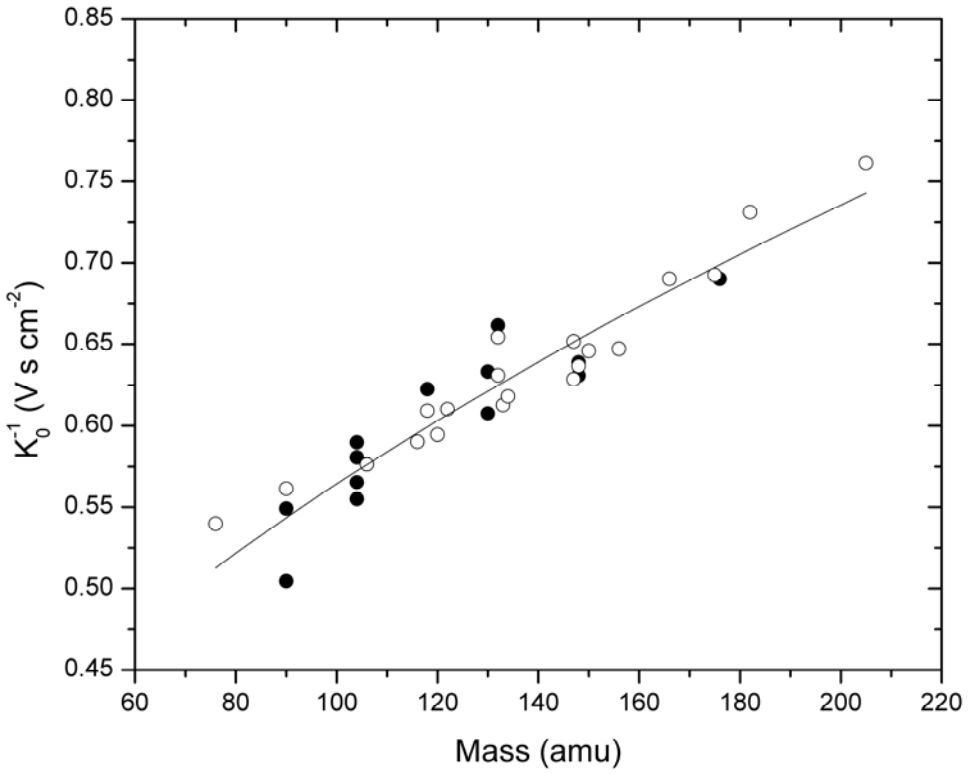
0.85
0.80
0.75
0.70
0.65
0.60
0.55
0.50
0.45
K_0^{-1} (V s cm^{-2})
60
80
100
120
140
160
180
200
220
Mass (amu)

values of the fitting parameters that produced the optimum fits as well as the various physical properties of the ion-neutral system given by the model.

Although all amino acids share a carboxylic acid and an amine group in common, there is a large variety in the R groups which can be aliphatic, contain aromatics, and/or contain carboxylic acid, amide, and mercapto groups, to name a few. Therefore, one might not expect to see a mass-mobility correlation among amino acids that is significantly better than the 20% level suggested by Griffin et al.[7] for structurally unrelated compounds. However, Figures 4 and 5 show that such a mass-mobility correlation does in fact exist. This statement is supported by the quality of the model fits to the mass-mobility data (R^2 values between 0.83 and 0.90; see Table 3). Considering both cases (i.e., N_2 and CO_2 drift gases), the worst observed deviation of the model from the measured mobilities is 7.2% with average deviations of 2.3% and 2.1% in the N_2 and CO_2 cases, respectively. The strength of the observed amino acid mass-mobility correlation is perhaps indicative that the amine and/or carboxylic acid groups are the dominant factors in determining the mobilities of these compounds and not the specific details of the R groups.

In a solvent solution of pH ~ 3, as in the present experiments, amino acids are likely to exist as cations with the positive charge (i.e., proton) at the amine group. As such, it is reasonable to assume that when the amino acid is ionized and released into the gas phase during the electrospray process, the positive charge remains at the amine group. Once in the gas phase, the ion is then likely to form hydrogen bonded 5- or 6-membered rings connecting the amine and carboxylic groups depending on whether the amine group is located on the α- or β-carbon (a 7- membered ring in the case of γ-amino-n-butyric acid which is the one amino acid considered here with the amine group on the γ-carbon).

Table 2. Model results for amino acids drifting in N_2 and CO_2

MW (amu)	N_2[a]				CO_2[b]			
	K_0 ($cm^2V^{-1}s^{-1}$)	ε (eV)	r_m (Å)	Ω ($Å^2$)	K_0 ($cm^2V^{-1}s^{-1}$)	ε (eV)	r_m (Å)	Ω ($Å^2$)
76	1.951	13.7	6.21	93.8	1.132	34.0	6.43	138.5
90	1.840	11.9	6.44	97.4	1.085	30.0	6.63	140.4
104	1.747	10.5	6.64	100.9	1.045	26.9	6.82	142.5
106	1.735	10.3	6.67	101.4	1.040	26.5	6.84	142.8
116	1.679	9.5	6.80	103.8	1.015	24.8	6.96	144.4
118	1.668	9.4	6.83	104.3	1.010	24.4	6.99	144.7
120	1.658	9.2	6.85	104.8	1.006	24.1	7.01	145.1
122	1.648	9.1	6.88	105.3	1.001	23.8	7.03	145.4
130	1.609	8.6	6.98	107.2	0.984	22.7	7.12	146.7
132	1.600	8.5	7.00	107.7	0.980	22.4	7.14	147.1
133	1.595	8.4	7.01	107.9	0.978	22.3	7.15	147.2
134	1.591	8.4	7.03	108.2	0.976	22.1	7.16	147.4
147	1.535	7.7	7.18	111.2	0.951	20.6	7.29	149.6
148	1.531	7.6	7.19	111.4	0.949	20.4	7.30	149.8
150	1.523	7.5	7.21	111.9	0.946	20.2	7.32	150.1
156	1.500	7.3	7.28	113.3	0.935	19.6	7.38	151.1
166	1.464	6.8	7.39	115.5	0.918	18.6	7.47	152.8
175	1.434	6.5	7.48	117.5	0.904	17.9	7.56	154.4
176	1.431	6.5	7.49	117.8	0.903	17.8	7.56	154.5
182	1.412	6.3	7.55	119.1	0.894	17.3	7.62	155.6
205	1.346	5.6	7.78	124.0	0.863	15.7	7.81	159.5

[a](r_0 = 2.56 Å, γ = 0.0004 Å/amu, a^* = 0.2). [b](r_0 = 2.92 Å, γ = 0.0000 Å/amu, a^* = 0.3).

The stability of a 5- or 6- (or even 7-) membered ring should result in fixing the positive charge to amine group rather than on other functional groups of the amino acid ion. This common charge location and ring structure may therefore lead to the observed indifference of the amino acid mass-mobility correlation to the specifics of the individual R groups.

One limitation in the fitting procedure was the fact the parameter a^* was only varied in a step-wise manner as described earlier. This simplification to the fitting procedure can be justified in part due to the fact that the value of $\Omega^{(1,1)^*}$, for a given T^* is a relatively slow varying function of a^* with a worst case variation (in the relevant region of the (T^*, a^*) plane; ~(1,0) → (8, 0.8)) of about ~6% between increments of a^* ($\Delta a^* = 0.1$). However, T^* itself is a function of a^* (equation 8) through the dependence of the potential depth on a^* (equation 7). Therefore, it is important to discuss the dependence of the "goodness of fit" to the mass-mobility data as a function of a^*.

Table 3 shows the χ_v^2 and R^2 values for the fits to the N_2 and CO_2 data sets as function of a^*. In the N_2 case, the quality of the fit was a relatively weak function of a^*, whereas the fit to the CO_2 data was strongly dependent on the value of a^*. However, the R^2 (χ_v^2) values for the CO_2 fits show a sharp peak (minimum) near $a^* = 0.3$ corresponding to the best fit to the CO_2 data. Therefore, in all three cases, it can be concluded that fitting with a finer interval of a^* would not have greatly altered the best fit parameter values and therefore would not significantly alter the outcome of the model's predictions.

Comparison of the of the model results for K_0, ε, r_m, and Ω for amino acids drifting in the different drift gases can provide insights into the physics of the ion-neutral interaction. Plots of these quantities for protonated amino acids drifting in N_2 and CO_2 drift gases

Table 3. χ_v^2 and R^2 values for the model fits to the amino acid mass-mobility curve as a function of a^*

a^*	N_2		CO_2	
	$\chi_v^{2\,a}$	R^2	$\chi_v^{2\,a}$	R^2
0	4.0	0.870	34.4	0.125
0.1	3.2	0.895	20.2	0.487
0.2	3.1	0.899	17.8	0.547
0.3	4.0	0.871	6.5	0.834
0.4	3.7	0.881	12.4	0.685
0.5	4.2	0.864	28.2	0.283
0.6	5.6	0.819	39.7	-0.010
0.7	6.5	0.788	45.9	-0.166
0.8	6.9	0.776	48.0	-0.221

[a] χ_v^2 values must be multiplied by 10^{-4}

are given in Figures 6, 7, 8, and 9 as a function of ion mass (over the mass range corresponding to the ions considered in this work) . The plot of K_0 in Figure 6 shows how drastically an ion's mobility can vary between different drift gases. Amino acid mobilities in N_2 are 50 – 75% larger than their mobilities in CO_2. Equation (11) shows that for a given temperature, the mobility is a function of μ, r_m and $\Omega^{(1,1)*}$. Since the reduced mass is a weak function of the ion mass for large polyatomic molecules (i.e., high mass) such as amino acids (constant if $m>>M$), the behavior of the mobitility is dominated by the interaction potential through r_m and $\Omega^{(1,1)*}$. Therefore, trends in mobility are best discerned by examining the parameters returned by the model that relate directly the interaction potential.

The potential depth of the CO_2-amino acid model is, on average, ~2.6× larger than the depth in N_2 (Figure 7). Equation 7 shows that the potential depth is directly proportional to the neutral polarizability. Therefore, the model results for ε coincide well with what one might expect based on the relative magnitudes of the neutral polarizabilities (α = 1.740 and 2.911 for N_2 and CO_2, respectively).

Figure 8 shows that the modeled r_m versus mass curves are roughly parallel. In the context of a hard sphere representation of the ion and neutral, r_m is given by the sum of the effective ion and neutral radii. Therefore, within this framework, the model results imply that the effective ion radii are essentially independent of the drift gas, as one might expect, even though no such constraint was enforced during the fitting procedure.

Figure 6. Model results for the reduced mobility, K_0, as a function of ion mass in N_2 (solid curve) and CO_2 (dash curve).

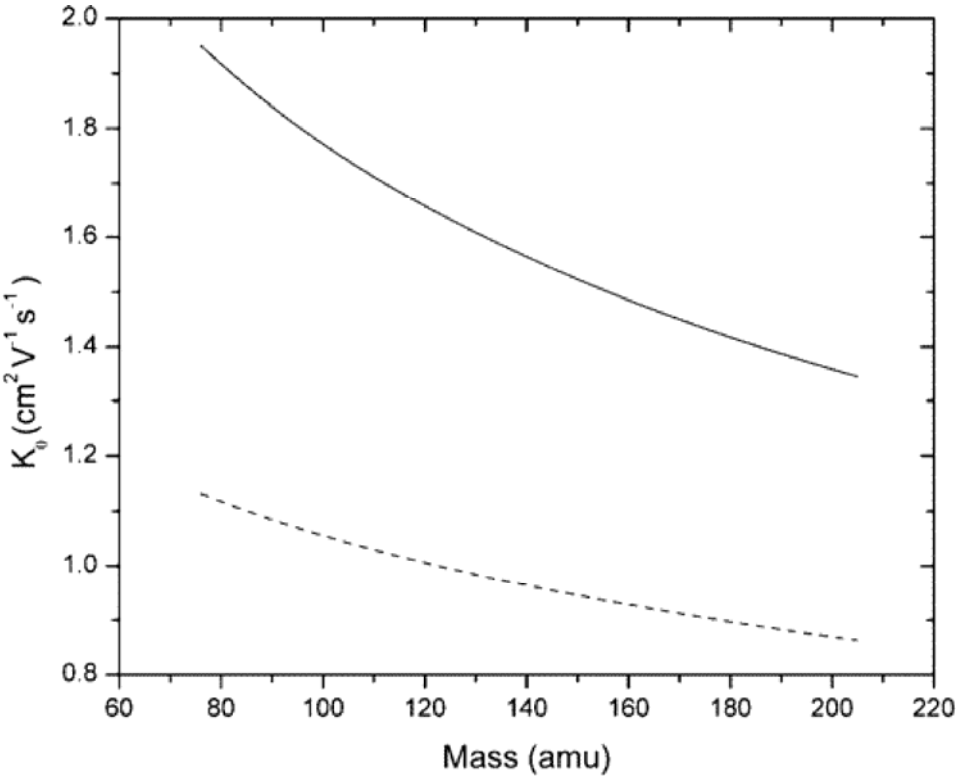

Figure 7. Model results for the potential depth, ε, as a function of ion mass in N_2 (solid curve) and CO_2 (dash curve).

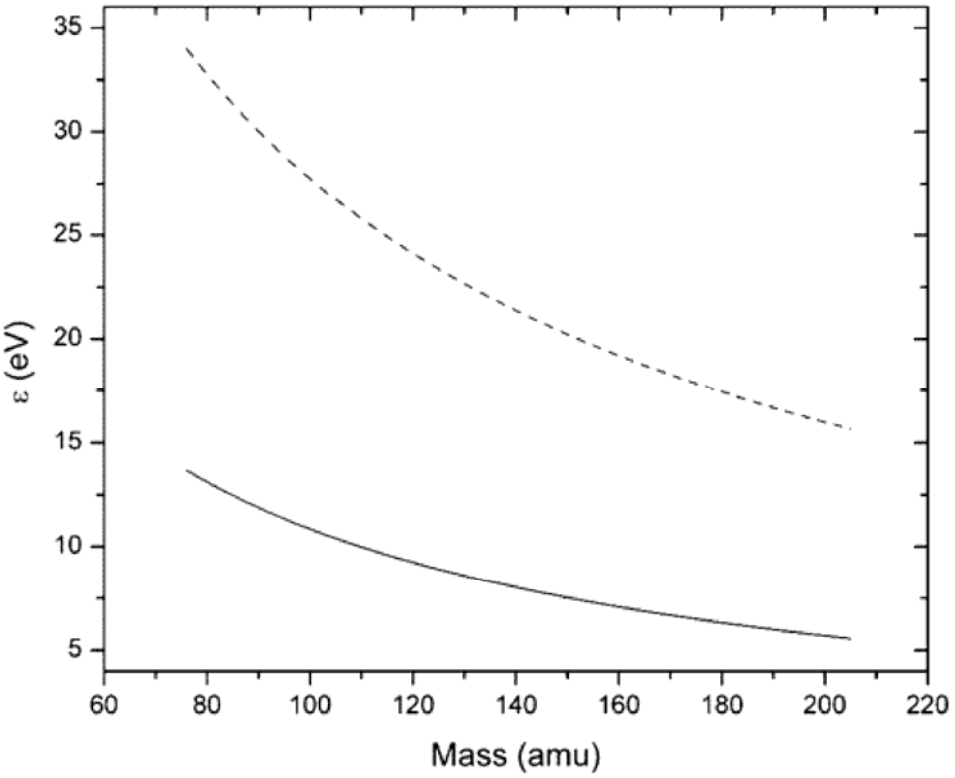

Figure 8. Model results for ion-neutral separation at the potential minimum, r_m, as a function of ion mass in N_2 (solid curve) and CO_2 (dash curve).

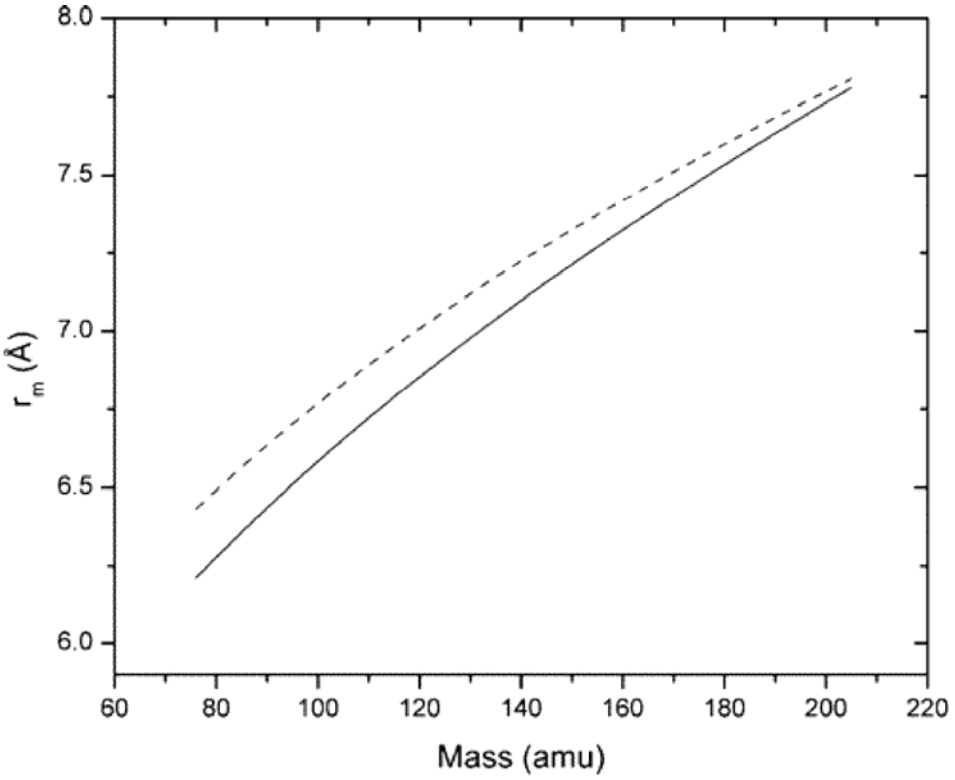

Figure 9. Model results for the collision cross section, Ω, as a function of ion mass in N_2 (solid curve) and CO_2 (dash curve).

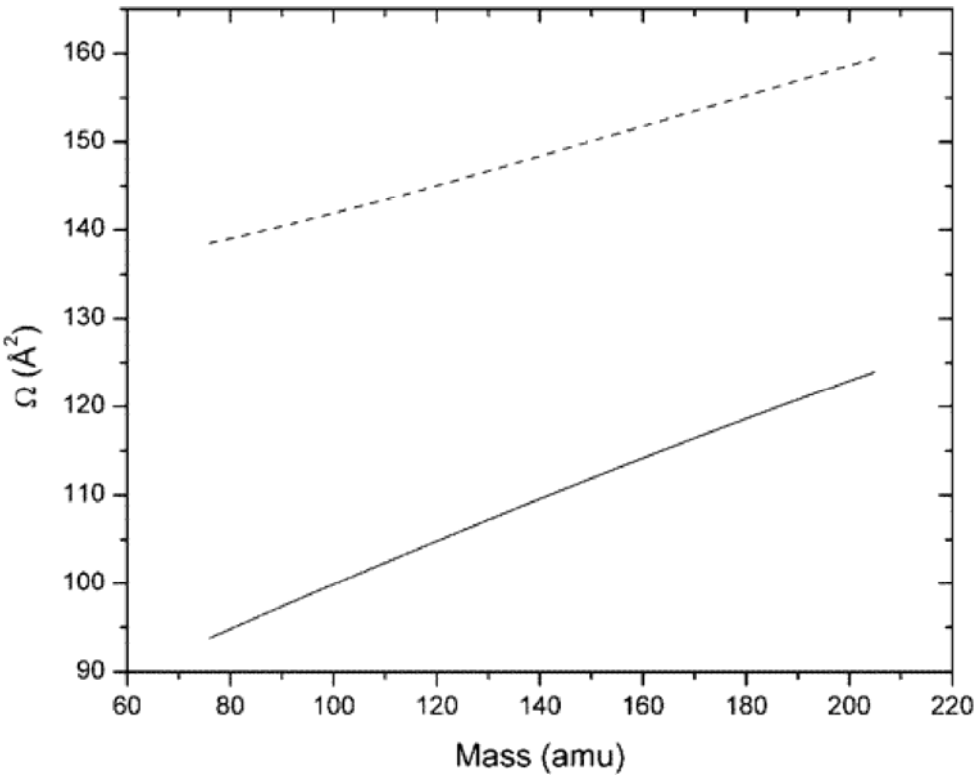

The cross section, Ω is given by $\pi r_m^2 \Omega^{(1,1)*}$ (eq 3), and so the results for the cross section will be interpreted in terms of the composite quantities. The values of r_m returned by the model are larger in CO_2 than in N_2. This is mirrored in the cross section through its quadratic dependence on r_m. Meanwhile, the influence of $\Omega^{(1,1)*}$ on Ω can be discerned in the magnitude of the CO_2 cross sections relative to those in N_2. $\Omega^{(1,1)*}$ is the direct result of a series of integrations over the interaction potential and increases with decreasing T^* (Mason et al.;[15] Figure 2), which is inversely proportional to ε. Therefore, the discrepancies in the potential well depths for protonated amino acids in each drift gas result in a significantly larger value of $\Omega^{(1,1)*}$ for amino acids in CO_2 than in N_2. This manifests itself in a similar result for the cross section.

Application of the (12,4) hard-core potential has not been restricted to the analysis of traditional IMS measurements. Recently, Guevremont et al.,[22] have applied the (12,4) hard-core potential to the analysis of electrospray ionization high-field asymmetric waveform spectroscopy (FAIMS) of amino acids in air. This work is of particular interest as the analysis was used to extract reduced ion mobilities as well as details of the ion-neutral (air) interaction through the defining parameters of the (12,4) hard-core potential. The analysis was performed by minimizing the root-mean-square deviation between calculated mobility ratios and those measured using FAIMS. In this minimization procedure, the parameters a^* and r_m were taken as independent fitting parameters. The authors present results for these parameters along with ε (determined from the obtained values of a^* and r_m; see equation 7) as well as the reduced mobilities for the amino acids measured. Since these data pertain to amino acid ions in air, and not the specific drift gases considered here, discussion will be restricted to the general trends in these data.

The mobilities presented by Guevremont et al.[22] for protonated amino acids in air generally decrease with increasing mass as expected and range between approximately 25% and 60% larger than those presented by Beegle et al.[1] for the same protonated amino acids in N_2. Although discrepancies between ion mobilities in different drift gasses are not surprising, it is interesting to note that the observed discrepancy demonstrates a roughly linear increase with increasing mass.

The general trend in the r_m values given by Guevremont et al.[22] is of decreasing r_m with increasing ion mass. This is in stark contrast to what is seen in this and other studies[8,9,17] and appears to be inconstant with what physical intuition would suggest. Over the range of ion masses represented in the Guevremont et al.[22] investigation (~130 amu), one would generally expect ion size to increase with increasing ion mass. Therefore, the location of the interaction potential minimum, r_m, which, if loosely interpreted as the center of mass separation between an ion and a molecule at the position of closest approach, should also increase with increasing mass. This is argument has been presented in more concrete terms earlier in section 3.1 where an expression for r_m was derived within the confines of a hard sphere model. This expression, given in equation 9 (equation 10, if an empirical correction is included), shows that r_m is a monotonically increasing function of ion mass. Although the hard sphere model represents a highly simplified view, it is difficult to imagine a situation that could produce an overall decreasing trend in r_m spanning an ion mass range of 130 amu.

Since ε is related to r_m in the manner prescribed in equation 7, the general trend in the Guevremont et al.[22] results for this parameter is to increase with increasing ion mass and is also contrary to what is seen in the present work and that of others[8,9,17]. It is interesting to note that K_0^{-1} is proportional to $r_m^2\ \Omega^{(1,1)*}$ (equation 11), and that $\Omega^{(1,1)*}$ increases as a

function of increasing ε [15]. Therefore, the intuitively unphysical behavior of r_m seen in the Guevremont et al.[22] data is presumably counteracted by the resulting reversal in the behavior of ε, and subsequently $\Omega^{(1,1)*}$, in such a way as to result in a reasonable behavior for K_0.

6.6. Conclusion

Reduced ion mobilities of 14 aboitic amino acids were determined via electrospray ionization-ion mobility spectrometry in both N_2, and CO_2 drift gases. Distinct differences in ion mobilities are demonstrated as a function of drift gases species. In terms of absolute magnitude, mobilities in N_2 were considerably larger than their CO_2 counterparts. Furthermore, a significant variation in the ion-to-ion mobility differences was observed in the two gases. In other words, noticeable differences in IMS separability were observed.

A (12,4) hard-core potential model for the ion-neutral interaction was applied to a combined data set of protonated amino acid mobilities (present work; Beegle et al.[1]). The model was fit to amino acid mobilites in N_2 and CO_2 as a function of ion mass. The quality of the fits indicated a strong correlation between the ion masses and their mobilities indicating that the amine and/or carboxylic acid groups dominate the mobility of these ions. Comparing the model results for amino acids in the three drift gases indicated that the polarizability of the neutral had a dominant effect on the ion-neutral interaction. Furthermore, the model indicated that the effective radius of the ion was essentially independent of the drift gas species, while the effective radius of the neutral was strongly influenced by its structural symmetry.

Work toward extending this model's application to different classes of organic molecules is underway. If mass-mobility correlations prove to be reasonably unique for different classes of organic compounds, one could use mass-mobility data to identify the family of compounds to which an unknown belongs in a manner similar to retention times in two dimensional gas chromatography.

6.7. Acknowledgment

This research was carried out at the Jet Propulsion Laboratory, California Institute of Technology, under a contract with the National Aeronautics and Space Administration (NASA), and was supported through NASA's Astrobiology Science and Technology Instrument Development, Planetary Instrument Development and Mars Instrument Development programs. The assistance of Professor H. H. Hill (Department of Chemistry, Washington State University, Pullman, Washington) in developing our IMS instrument is gratefully acknowledged.

6.8. References

(1) Beegle, L.W.; Kanik, I.; Matz, L.; Hill, H. H. *Anal. Chem.* **2001**, 73, 3028-3034.

(2) Beegle, L.W.; Kanik, I.; Matz, L.; Hill, H. H. *Int. J. Mass Spectrom.* **2002**, 216, 257-268.

(3) Kvenvold, K.; Lawless, J.; Pering, K.; Peterson, E.; Flores, J.; Ponnampe, C.; Kaplan, I. R.; Moore, C. *Nature* **1970**, 228, 923-926.

(4) Oro, J.; Gibert, J.; Lichtens, H.; Wikstrom, S., Flory, D.A. *Nature* **1971**, 230, 105.

(5) Cronin, J. R.; Moore, C. B. *Science* **1971**, 172, 1327-1329.

(6) Cronin, J. R.; Pizzarello, S. *Ad. Space Res.* **1983**, 3, 5-18.

(7) Griffin, G. W.; Dzidic, I.; Carroll, D. I.; Stillwell, R. N.; Horning, E. C. *Anal. Chem.* **1973**, 45, 1204-1209.

(8) Berant, Z.; Karpas, Z. *J. Am. Chem. Soc.* **1989**, 111, 3819-3824.

(9) Karpas, Z.; Berant, Z. *J. Phys. Chem.* **1989**, 93, 3021-3025.

(10) Illenseer, C.; Löhmannsröben, H. G. Phys. *Chem. Chem. Phys.* **2001**, 3, 2388-2393.

(11) Asbury, G. R.; Hill, H. H. *J. Micro. Sep.* **2000**, 12, 172-178.

(12) Wu, C.; Siems, W. F.; Asbury, G. R.; Hill, H. H. *Anal. Chem.* **1998**, 70, 4929-4938.

(13) Revercomb, H. E.; Mason, E. A. *Anal. Chem.* **1975**, 47, 970-983.

(14) Hirschfelder, J. O.; Curtiss, C. F.; Bird, R. B. Molecular Theory of Gases and Liquids, John Wiley: New York, **1964**, Chapter 8.

(15) Mason, E. A.; O'Hara, H.; Smith, F. J. *J. Phys. B: Atom. Molec. Phys.* **1972**, 5, 169-176.

(16) Mason, E. A. In Plasma Chromatography; Carr, T. W., Ed.; Plenum Press: New York **1984**, Chapter 2.

(17) Berant, Z.; Karpas, Z.; Shahal O. *J. Phys. Chem.* **1989**, 93, 7529-7532.

(18) Berant, Z.; Shahal, O.; Karpas, Z. *J. Phys. Chem.* **1991**, 95, 7534-7538.

(19) CRC Handbook of Chemistry and Physics 83rd Edition; Lide, D. H., Ed.-in-Chief; CRC Press LLC: Boca Raton **2002**.

(20) Asbury, G. R.; Hill, H. H. *Anal. Chem.* **2000**, 72, 580-584.

(21) Matz, L. M.; Hill, H. H.; Beegle, L. W.; Kanik, I. *J. Am. Soc. Mass Spectrom.* **2002**, 13, 300-307.

(22) Guevremont, R.; Barnett, D. A.; Purves, R. W.; Viehland, L. A. *J. Chem. Phys.* **2001**, 114, 10270-10277